Reserve Capability Assessment Considering Correlated Uncertainty in Microgrid

Sohail Khan, *Student Member, IEEE*, Wolfgang Gawlik, and Peter Palensky, *Senior Member, IEEE*

***Abstract*—This paper presents a novel approach of assessing the required reserve capability in order to meet the forecast uncertainty dynamics in microgrid. The historical data of forecast variables is used to generate energy balance scenarios. The dynamics of these scenarios are represented as instances between capacity, ramp-rate and ramp-duration variables. A polytopic model is used to enclose these instances with its surface defining the worst case scenarios. This approach captures the correlated nature of the dynamics and provides a compact representation. In relevance, the capability of the generators and the power import from the grid are modeled as convex envelopes. A vertex based method is proposed that allocates the polytope among the resource envelopes. During this process, the operational cost is minimized while considering the resource location and the network constraints. The proposed method is examined for a microgrid test case based on the CIGRE medium voltage network. The results show new insights in the allocated demand and reserve capabilities. As an additional result, it is observed that the reserve requirements can be decreased by allocating reserves for each time instance separately as compared to the fixed percentage of load approach.**

***Index Terms*—Microgrid, Reserve, chance constrained, optimization, Markov chain, Monte Carlo, uncertainty, polytope.**

NOMENCLATURE

A. Indices

i	Index of the generator, from 1 to N.
t	Time index, from 1 to T.
s	Monte Carlo sample index, from 1 to S.
f	Index of forecast cluster, from 1 to F.
u	Index of uncertain variable, from 1 to n_δ.
d	Index of generator power, from 1 to D.
m	Index of generator ramp-up rate, from 1 to M.
n	Index of generator ramp-down rate, from 1 to N.
j	Index of polytope section, from 1 to C.
k	Vertex index of j^{th} sub-polytope , from 1 to V_j.

B. Sets and Parameters

$\overline{P_i}$	Max. active power rating of generator i [MW].
$\overline{Q_i}$	Max. reactive power rating of generator i [Mvar].
$\underline{P_i}$	Min. active power rating of generator i [MW].
$\underline{Q_i}$	Min. reactive power rating of generator i [Mvar].
$(1-\beta)$	Confidence in the probabilistic result.
$(1-\epsilon)$	Probability of the constraint satisfaction.
L_f	Probabilistic limits on the forecast cluster f.
Δ, Δ_i	Uncertain demand, generator flexibility envelope.
$\overline{\delta_u}, \underline{\delta_u}$	Max. and min. values of uncertain variable u.
$\epsilon_{\Delta P}$	Minimum ramp-rate tolerance [MW/h].
k_i	Temperature power slope of generator i [°F/kW].
τ_i	Thermal time constant of generator i [min].
w	Duration of ramp [min].
$\underline{L_i},\ H_i$	Low, high thermal stress limit of generator i [°F].
$\overline{R_i^+}$	Max. ramp-up rate of generator i [MW/h].
$\overline{R_i^-}$	Max. ramp-down rate of generator i [MW/h].
G_{ab}	Conductance of line between bus a and b.
B_{ab}	Susceptance of line between bus a and b.
P_{Da}	Real power demand at bus a [MW].
Q_{Da}	Reactive power demand at bus a [Mvar].
P_{loss}	Transmission loss [MW]
S_{symb}	Set of all the buses, generator buses and transmission lines for symb = B,G,L in the network.
$\overline{P_{L_{ab}}}$	Max. active power capacity of line ab [MW].
$\underline{P_{L_{ab}}}$	Min. active power capacity of line ab [MW].

C. Variables

ΔP^t_{symb}	Uncertainty in the demand, wind and PV power for symb $= D, w, PV$ during t^{th} hour.
ΔP^t	Lumped uncertainty in microgrid during t^{th} hour.
P_i^d	The d^{th} power of generator i.
$R_{i,m}^+$	The m^{th} ramp-up rate of generator i.
$R_{i,n}^-$	The n^{th} ramp-down rate of generator i.
P_i^j	Active power of i^{th} generator against j^{th} demand.
x_j	The j^{th} demand value in microgrid.
$S_j(\Delta)$	The j^{th} uncertainty sub-polytope of polytope Δ.
$y_j^k,\ z_j^k$	The k^{th} vertex coordinates of $S_j(\Delta), 1 \cdots V_j$.
H_i^j	Half-space coefficients of $S_j(\Delta_i)$.
$r_i^k,\ d_i^k$	The k^{th} vertex coordinates of $S_j(\Delta_i), 1 \cdots V_j$.
P_i^t	Active power of i^{th} generator at time t.
R_i^t	Reserve contribution of i^{th} generator.
Q_i^t	Reactive power of i^{th} generator at time t.
$e_i,\ f_i$	Real and imaginary values of i^{th} bus voltage.
S_i^t	Thermal stress state of generator i.
$a_i,\ b_i$	Cost coefficients of generator i.

Manuscript received April 14, 2015; revised August 08, 2015 and October 11, 2015; accepted October 30, 2015. Date of publication December 03, 2015; date of current version March 18, 2016. Paper no. TSTE-00286-2015.

S. Khan is with Complex Energy Systems, Department of Energy, Austrian Institute of Technology (AIT) GmbH, 1210 Vienna, Austria (e-mail: sohail.khan.fl@ait.ac.at).

W. Gawlik is with the Institute for Energy Systems and Electrical Drives, Vienna University of Technology, 1040 Vienna, Austria.

P. Palensky is with the Department of Electrical Sustainable Energy, Delft University of Technology, 2600 Delft, The Netherlands.

Color versions of one or more of the figures in this paper are available online at http://ieeexplore.ieee.org.

Digital Object Identifier 10.1109/TSTE.2015.2498143

I. Introduction

THE increase in the integration of Renewable Energy Sources (RES) in electric distribution system has introduced critical operational challenges in the recent years. The underlying reason is the uncertain and volatile nature of the power generated from RES [1]. This has increased the reserve flexibility requirements in the system. Provision of the distribution side resources providing flexible reserve services can propose a local and cost effective solution [2]. Various energy management strategies are discussed in the literature to enable the active participation of such resources. The microgrid is considered as an attractive choice among them [3]. It provides a platform for aggregating the reserve flexibility from resources and can perform their coordinated control. An overview of the control and reserve management strategies in microgrid is discussed in [4]. In [5], a stochastic energy and reserve scheduling method is proposed considering the demand response in the microgrid. While in [6], authors have used artificial neural networks for the forecasting and used the results for the reserve quantification in microgrid. These studies focus on an interval based approach for the reserve allocation. In this paper, a more holistic approach is taken by modeling the uncertainty dynamics. This consideration leads to the assessment of required reserve capability in microgrid and is used as a reference during resource allocation.

The forecasting methods can be classified as linear/nonlinear regression, probabilistic time series and neural networks based methods. Among them, the probabilistic time-series based method is used in this paper. Ref. [7] uses the Markov chain to model time series dynamics of the uncertain variable. It is used here to model the temporal aspect of forecast uncertainty. The spatial aspect is taken into account by clustering the forecast data. For this purpose, a binning strategy based on the magnitude of forecast data is used. Other methods like $k-means$ [8] can be used similarly. The spatio-temporal probabilistic model is used to generate scenarios for a day ahead power balance forecast in microgrid. The number of scenarios is selected using chance constrained optimization theory [9]. It defines the number of scenarios for a desired level of confidence against uncertainty.

The dynamics of scenarios can be represented by the flexibility metrics. In [10] and [11], the first-order dynamics are modeled in terms of power capacity, ramp-rate and ramp-duration variables. Authors have used an interval based approach that results in a hyper-rectangular model. The vertices of rectangle represents the worst case scenarios and is used for the reserve allocation. This approach can be useful for large systems as it reduces the computational burden. However, it considers the worst case ramp-rate for the maximum capacity and ramp-duration values. Maintaining such margins can lead to a safer operation of the system. However, in case of the microgrid with limited resources, it may result in additional costs. While analyzing the uncertainty dynamics, it is observed that the ramp-rate and ramp-duration are correlated with the capacity values. This correlation cannot be represented by the interval based methods. In relevance, compact geometric models are of interest. The application of such models has been reported in the recent literature. In [12], authors have modeled the available transfer capacity in the multi-area networks using a geometric approach. While in [13], a polyhedral form models the region for real time dispatchability problem. These studies further encouraged the use of geometric models.

Among the compact envelope modeling approaches, the ellipsoidal uncertainty model is discussed in [14]. It is of interest as an ellipse can be represented by few parameters. However, in order to complete the envelope it encloses the negative ramp-duration region, whereas, the duration is a non-negative variable. The intersection of an ellipse with the half space extending along positive ramp duration results in a polyhedral structure. Thus the advantage of using ellipse is no more valid. In comparison, polytope is a compact representation of the uncertainty space that we use in this work.

The allocation of reserves according to the uncertainty dynamics requires the modeling of resource capability in relevance. The controllable generation resources considered here are the Distributed Generators (DGs) and the power import from the main grid. Ref. [15] and [16] discusses the dynamic ramp-rate model of generator. In these papers, authors have discussed the economic advantage of using dynamic ramp-rate as function of the thermal stress on rotor. The study reveals that while operating a generator with-in its thermal limits the ramp-rate can be defined as a dynamic value without causing additional costs. Using this work, the generator capability is modeled by a convex envelope among the dynamics variables. Demand polytope is then allocated among the generator envelopes in the resource allocation process. A vertex based allocation method is presented for this purpose. It optimizes for the cost while considering the resource and network constraints. The assumptions considered are: 1) the probabilistic distribution function of the forecast error is not available therefore a non-parametric approach is used; 2) the generators are operated within thermal limits therefore the depreciation of machine is not considered; and 3) polytopes model the forecast uncertainty and generator capability with sufficient compactness.

The uncertainty dynamics considerations can be particularly relevant to the microgrids operating at medium voltage (MV) level e.g., Bornholm island microgrid [17]. Other microgrid projects and their control strategies are reviewed in [18]. The microgrid test case selected in this work is based on CIGRE MV benchmark model [19], [20].

The main contributions are summarized as,

- A convex polytope approximation for modeling the uncertain power balance dynamics resulting in a compact representation.
- A vertex based geometric allocation method that allocates the uncertain demand polytope between the generator capability envelopes. The economic optimization considers the resource and network operational constraints.

The organization of paper is shown in Fig. 1. Section II presents the modeling of uncertain power balance dynamics and the generator capability. Section III discusses the resource allocation methods. Section IV discuss the test case demonstration of the proposed approach. In the end, conclusion and future work is discussed in Section V.

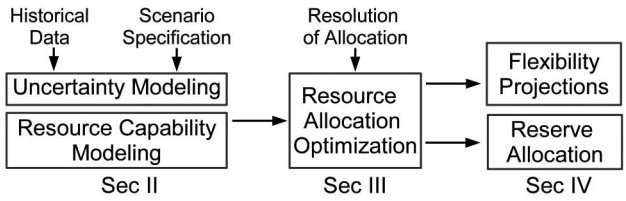

Fig. 1. Overview of the method presented in the paper.

II. Modeling

This section models the desired and the available flexibility in meeting the real power demand dynamics in the microgrid. From Sec. II-A to II-C, a methodology is proposed to model the power balance dynamics. The operational capability of the generator is modeled in Sec. II-D.

A. Stochastic Constraint Formulation

The forecast variables considered here are the load, real power generated from the wind-farm and PV. The lumped uncertainty of the power balance in microgrid is given as,

$$\Delta P^t = \Delta P_D^t - \left(\Delta P_w^t + \Delta P_{PV}^t\right). \tag{1}$$

The power balance equation is,

$$\sum_{i=1}^{N} P_i^t = P_D^t - \left(P_w^t + P_{PV}^t\right) + P_{\text{loss}}. \tag{2}$$

The operational limit constraint of the generator i is,

$$\underline{P_i} \leq P_i^t \leq \overline{P_i}. \tag{3}$$

The spinning reserve constraint is given as,

$$R_i^t \leq \overline{P_i} - P_i^t, \tag{4}$$

$$\sum_{i=1}^{N} R_i^t \geq \Delta P^t. \tag{5}$$

Eq. 4 constrains the reserve contribution of generator i within the power limits. While, Eq. 5 states that the available spinning reserve should at least meet the lumped uncertainty.

The stochastic nature of uncertainty in Eq. 5 makes the constraint probabilistic. The generic structure of optimization problem involving probabilistic constraint is given as,

$$\begin{aligned} \min_{x\in\mathbb{R}^{n_x}} \quad & J(x), \\ \text{s.t.:} \quad & \mathbb{P}\left(\delta \in \Delta \mid \max_{s=1,\ldots,M} g_s(x,\delta) \leq 0\right) \geq (1-\epsilon). \end{aligned} \tag{6}$$

Here, $J\colon \mathbb{R}^{n_x} \to \mathbb{R}$ is the objective function and $g_s\colon \mathbb{R}^{n_x} \times \Delta \to \mathbb{R}$ are M inequality constraint functions involving the uncertainty $\delta \in \Delta \subseteq \mathbb{R}^{n_\delta}$. Δ corresponds to the uncertainty envelope from which the δ instances are drawn. Any constraint satisfying Eq. 6 is referred as ϵ level feasible solution [9]. This value is related to the number scenarios (S) generated in order to approximate the uncertainty envelope Δ. The large value of S implies greater chance for the inclusion of the rare forecast error scenarios.

Among the various stochastic optimization methods, chance constrained optimization is selected for this work. The key benefit of this method is that it does not require the information about the probability distribution of the stochastic variables and their mutual correlation. By using this method a set of worst case scenarios is generated with a certain degree of confidence. For a given constraint satisfaction level $(1-\epsilon) \in (0,1)$ and confidence $(1-\beta) \in (0,1)$, S is selected according to [9],

$$S \geq \frac{1}{\epsilon}\left(\frac{e}{e-1}\right)\left(\ln\left(\frac{1}{\beta}\right) + 2 * n_\delta - 1\right). \tag{7}$$

Here, e is the Euler constant and n_δ is the number of uncertain variables. This approach yields a probabilistic level of accuracy and confidence in quantifying the uncertain region.

For the un-correlated uncertain variables, Δ can be represented by a Bounding-Box (BB) $B^* := \times_{u=1}^{n_\delta}\left[\underline{\delta_u}, \overline{\delta_u}\right]$. Here, B^* is the extremum of uncertain variable δ_u as discussed in [9]. Thus Eq. 6 becomes,

$$\begin{aligned} \min_{x\in\mathbb{R}^{n_x}} \quad & J(x), \\ \text{s.t.:} \quad & \max_{s=1,\ldots,M} \quad \max_{\delta\in B^*\cap\Delta} \quad g_s(x,\delta) \leq 0. \end{aligned} \tag{8}$$

Here, M inequality constraints are satisfied for the maximum values of the uncertainty δ which are the vertices of B^* [10]. In this work, a convex envelope in the form of polytope is used to model the uncertainty region. It yields to,

$$\begin{aligned} \min_{x\in\mathbb{R}^{n_x}} \quad & J(x), \\ \text{s.t.:} \quad & \max_{s=1,\ldots,M} \quad \max_{\delta\in\Delta} \quad g_s(x,\delta) \leq 0. \end{aligned} \tag{9}$$

Here, the inequality constraint formulation is for the uncertainty (δ) within the envelope (Δ). Similarly, Eq. 5 must be satisfied for $\Delta P^t \in \Delta$. The Δ is obtained using number of scenarios from Eq. 7 and is therefore probabilistic. Hence, Eq. 5 is given as,

$$\mathbb{P}\left(\sum_{i=1}^{N} R_i^t \geq \Delta P^t\right) \geq (1-\epsilon). \tag{10}$$

Eq. 10 states that if the reserve is sufficient to address the uncertainty envelope Δ constructed using S scenarios, then the reserve constraint is satisfied with $(1-\epsilon)$ probability.

B. Uncertainty Scenario Generation

In order to combine the uncertainty from variables, it is taken as the percentage deviation from the forecast value. While analyzing the historical data, it is observed that the % error is related to the forecast level. Such that, high forecast level has a smaller % error as compared to low level. Thus, a single probabilistic model cannot be applied to represent error in the forecast values. Therefore, the forecast data is divided into clusters. A binning strategy based on the magnitude is used to categorize the forecast data in clusters. It is assumed that

the probability distribution of the error in each cluster is not known. Hence, a non-parametric probability density approach is applied. The empirical Cumulative Distribution Function (eCDF) from [10] used in this work.

The temporal correlation between the forecast time-series data is captured by a second order Markov chain. For this purpose, the Transition Probability Matrix (TPM) is derived using work in [7]. The three dimensional matrix captures the probability of an error state given the two previous states. An algorithm considering the spatio-temporal aspects is presented in Alg. 1. It is used to generate the power balance scenarios in microgrid.

Algorithm 1. Uncertainty Modeling

1 Categorize the forecast data in F clusters based on the magnitude;
2 Obtain eCDF of the forecast error in each cluster;
3 **for** $f := 1 \cdots F$ **do** *(Forecast error limit loop)*
4 | Sample the eCDF of f^{th} cluster S times;
5 | Save boundary values as stochastic error bounds L_f;
6 **end**
7 Model the forecast error time-series correlation by deriving the Transition Probability Matrix (TPM) for second order Markov chain;
8 **for** $s := 1 \cdots S$ **do** *(Forecast realizations loop)*
9 | Assume initial states of error at $t = 1, 2$;
10 | **for** $t := 3 \cdots T$ **do** *(Time periods loop)*
11 | | Use uniform random number generator to generate a probability value;
12 | | Find the t^{th} error state by checking the probability value on the axis defined by the previous two error states on TPM;
13 | | Bound the t^{th} state by the limits of corresponding forecast cluster $h(t)$ given as $L_{h(t)}$;
14 | **end**
15 **end**

C. Uncertainty Envelope Model

Various compression algorithms are used in the literature for extracting the dynamics of a curve. Algorithms like box-car, averaging and Swinging Door Algorithm (SDA) are discussed in [21]. Inspired from [10], SDA is selected for this work. The working principle of this algorithm is shown in Fig. 2. It is applied to the scenarios and it leads to pivot-points. Each pivot-point defines the dynamics in terms of three variables, the capacity $(\Delta P = \pi)$, ramp-rate (ρ_{1-3}) and the ramp-duration (μ). The sensitivity of the approach is based on the tolerance $\epsilon_{\Delta P}$. It is related to minimum ramp-rate limit of the participating generators. A polytope is modeled to enclose the pivot-points. It extends the probabilistic confidence from Eq. 7 to the surface of polytope. The consideration of polytope as a representative of uncertainty dynamics results in the satisfaction of constraint in Eq. 10.

A polytope is a convex and compact set given as an intersection of finite number of closed half-spaces. The $\mathcal{H}$ representation or the hyper-plane definition is given as,

$$\mathcal{P} = \{x \in \mathbb{R} \mid P^x x \leq P^c\}. \tag{11}$$

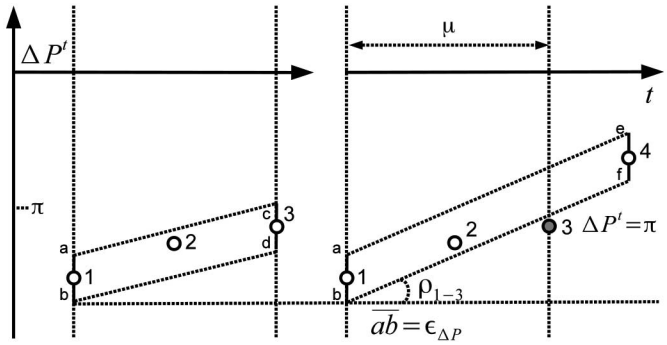

Fig. 2. A data compression algorithm called "swinging door" is re-plotted from [10]. It is used to extract the first order dynamics of the curve. The sampled values of lumped uncertainty ΔP^t are shown here by the points $1-4$. With each iteration a parallelogram is drawn with the desired sensitivity $\epsilon_{\Delta P}$. The parallelogram is checked to contain all the previous points. Which is true in case of $abcd$. However, at $t = 4$ the point 3 lies outside $abef$. The point 3 is termed as the pivot point. It is represented by magnitude (π), ramp-rate (ρ_{1-3}) and the ramp-duration (μ).

It can also be defined by the $\mathcal{V}$ definition [22],

$$\mathcal{P} = \left[x \in \mathbb{R} \mid x = \sum_{i=1}^{\upsilon_P} m_i V_P^i, m \in [0,1], \sum_{i=1}^{\upsilon_P} m_i = 1 \right] \tag{12}$$

Here, $V_P^{(i)}$ is the i^{th} vertex of $\mathcal{P}$ and υ_P is the total number of vertices (pivot-points). The polytope $\mathcal{P}$ can be divided into two sub-polytopes based on the sign of power. The sub-polytope having non-negative value of the power represents local demand dynamics. These dynamics needs to be allocated among the generators in microgrid. The other sub-polytope models the dynamics of power export to the grid. Here, demand polytope is focused and is referred as Δ.

The vertices of Δ defines the worst case scenarios of power demand. The limited number of vertices may not be sufficient for the resource allocation process discussed in Sec. III. Therefore, Alg. 2 is used to find the required number of points on the surface of Δ. The process sections Δ into C sub-polytopes along the demand axis. The coordinates of the sub-polytope are given as $[x_j \; y_j^k \; z_j^k]$. Here, x_j is the j^{th} capacity/power among C capacity values and (y_j^k, z_j^k) is the k^{th} vertex among V_j vertices. V_j vertices of $S_j(\Delta)$ represents the maximum ramp-rate and ramp-duration values for the demand x_j.

Algorithm 2. Sectioning of polytope (Δ)

1 Compute the bounding box around Δ;
2 Based on desired spacing divide the power axis interval into C equidistant points (x_j);
3 **for** $j := 1 \cdots C$ **do** *(Polytope sectioning loop)*
4 | For each x_j define an orthogonal hyper-plane;
5 | Intersect Δ with the hyper-plane leading to polygon $S_j(\Delta)$;
6 **end**

D. Generator Capability Modeling

The generator capability modeling is used to assess the maximum flexibility that can be obtained in terms of the active power

ramp-rate. The fatigue curves from the generator manufacturer represents thermal stress on the turbine shaft as a function of the ramp-rate. Generator ramp-rate limits are transformed to thermal stress elastic limits from the fatigue curve data.In [16], the thermal state of the generator is modeled as function of the previous thermal state (decaying term) and thermal contribution due to the ramp process (growth variable). The fatigue curves assume thermal equilibrium at initial point and a constant ramp-rate [15]. Therefore, the decaying term is neglected resulting in a simplified form given as,

$$S_i^t = k_i\tau_i\left(1-e^{-w/\tau_i}\right)\left[P_i(t)-P_i(t-1)\right]/w. \tag{13}$$

In terms of ramp-up rate (RU_i), the shift in power is,

$$P_i(t)-P_i(t-1) = wRU_i\ , \tag{14}$$

leading to the thermal state of generator given as,

$$S_i = k_i\tau_i RU_i\left(1-e^{-w/\tau_i}\right). \tag{15}$$

Same approach can be used for the ramp-down rate (RD_i) as well. The thermal limits of the stress in both directions are,

$$-L_i \le S_i \le H_i, \quad i = 1\cdots M. \tag{16}$$

The per-hour maximum ramp-up and ramp-down rate $(\overline{R_i^+},\ \overline{R_i^-})$ are obtained by solving Eq. 15 for thermal limits and ramp duration $(w = 60$ min$)$ given as,

$$H_i = k_i\tau_i\overline{R_i^+}\left(1-e^{-60/\tau_i}\right), \tag{17}$$

$$L_i = k_i\tau_i\overline{R_i^-}\left(1-e^{-60/\tau_i}\right). \tag{18}$$

In the next step, equidistant points of the power (P_i^d), ramp-up $(R_{i,m}^+)$ and ramp-down rate $(R_{i,n}^-)$ of generator i are taken from the intervals,

$$\underline{P_i} \le P_i^d \le \left(\overline{P_i}-\overline{R_i^+}\right), 0 \le R_{i,m}^+ \le \overline{R_i^+}\ , \tag{19}$$

$$\overline{P_i} \ge P_i^d \ge (\underline{P_i}+\overline{R_i^-}), 0 \le R_{i,n}^- \le \overline{R_i^-}. \tag{20}$$

Eq. 19 describe the range for selecting the power and ramp-up rate that can be assigned to generator i. Similarly, Eq. 20 describe interval for the ramp-down rate. Maximum ramp duration (w) is calculated for each pair of power (P_i^d) and ramp-up rate $(R_{i,m}^+)$ by solving,

$$\max \quad w\ , \tag{21a}$$

$$\text{s.t.}: \quad k_i\tau_i R_{i,m}^+\left(1-e^{-w/\tau_i}\right) \le H_i\ , \tag{21b}$$

$$\left(R_{i,m}^+ w + P_i^d\right) \le \overline{P_i}\ . \tag{21c}$$

The point $[P_i^d\ R_{i,m}^+\ w]$ defines a boundary instance in generator envelope for the positive ramp domain. Similarly maximum ramp-duration is found for each pair of the power (P_i^d) and ramp-down rate $(R_{i,n}^-)$ by solving,

$$\max \quad w, \tag{22a}$$

$$\text{s.t.}: \quad k_i\tau_i R_{i,n}^-\left(1-e^{-w/\tau_i}\right) \ge L_i\ , \tag{22b}$$

$$\left(P_i^d - R_{i,n}^- w\right) \ge \underline{P_i}\ . \tag{22c}$$

The process is repeated for all pairs of capacity and ramp-up/down values leading to points in the space. A convex envelope (Δ_i) then encloses these points defining the capability limits of generator i.

III. Resource Allocation

In this section, the decomposition of uncertain demand envelope (Δ) among the generator capability envelopes (Δ_i) is performed. The area of computational geometry provides insights in the space allocation methods [23]. One of the method is to model the allocation process as an optimization problem with Δ defined in the hyper-plane representation. It is found that the corresponding allocation process involves non-convex scaling along ramp-rate and ramp-duration axes. While, Minkowski sum can be relevant for the demand allocation process. In comparison, a vertex based allocation method is developed. It facilitates the modeling of constraints on individual variables. The allocation of Δ among resources is a deterministic process. During which, the power import from the main grid is used as a slack resource. Δ is decomposed in two steps, the demand and dynamics allocation.

A. Demand Allocation

In this process, the range of the Δ along power axis is divided into desired number of equidistant points C. Here, each point is a demand value termed x_j. Each x_j is dispatched among the resources by solving,

$$\min \quad \sum_{i=1}^{N}\left[a_i P_i^j + b_i (P_i^j)^2\right], \tag{23a}$$

$$\text{s.t.}: \quad \forall\ i = 1\cdots N,\ j = 1\cdots V_j$$

Power balance constraint,

$$\sum_{i=1}^{N} P_i^j \ge x_j\ , \tag{23b}$$

Generator active power limits,

$$\underline{P_i} \le P_i^j \le \overline{P_i}, i \in S_G\ , \tag{23c}$$

Generator reactive power limits,

$$\underline{Q_i} \le Q_i^j \le \overline{Q_i}, i \in S_G\ , \tag{23d}$$

Power flow equations,

$$P_{Ga} - \sum_{b\in S_B}\left[e_a(e_bG_{ab}-f_aB_{ab})+f_a(f_bG_{ab}+e_bB_{ab})\right] = P_{Da}$$

$$Q_{Ga} - \sum_{b\in S_B}\left[f_a(e_bG_{ab}-f_aB_{ab})-e_a(f_b^tG_{ab}+e_bB_{ab})\right] = Q_{Da}$$

$$a \in S_B\ i.e.,\ \forall a \notin S_G \Rightarrow P_{Ga},\ Q_{Ga} = 0\ , \tag{23e}$$

Transmission line constraint,

$$\underline{P_{L_{ab}}} \le P_{L_{ab}} \le \overline{P_{L_{ab}}}\ ,$$

where,

$$P_{L_{ab}} = \left[e_a^2 + f_a^2 - e_ae_b - f_af_b\right]G_{ab} + (e_af_b - e_bf_a)B_{ab}\ ,\ ab \in S_L\ , \tag{23f}$$

Bus voltage limit constraint,

$$\underline{V_a}^2 \leq \left(e_a^2 + f_a^2\right) \leq \overline{V_a}^2, \quad a \in S_B. \tag{23g}$$

The constraints in Eq. 23c and 23d ensures the consideration of generator active and reactive power limits. While, the transmission line and voltage limit constraints in Eq. 23f and 23g incorporates the location and operational aspects.

B. Dynamics Allocation

The polytope Δ is sectioned at each demand value x_j using Alg. 2 resulting in C sub-polytopes $(S_j(\Delta))$. Here, the vertices of $S_j(\Delta)$ represents the ramp-rate and ramp-duration. In the first step, the polytope of each generator Δ_i is sectioned at the assigned power P_i^j leading to the sub-polytopes $S_j(\Delta_i)$. The allocation is then performed for each vertex k of $S_j(\Delta)$, where $k = 1 \cdots V_j$. The k^{th} vertex of $S_j(\Delta)$ is given as $[y_j^k \; z_j^k]$. The corresponding generator vertices $(g_i^k = [r_i^k \; d_i^k])$ are found by solving,

$$\min \quad \sum_{i=1}^{N} \left[a_i(r_i^k d_i^k) + b_i(r_i^k d_i^k)^2\right], \tag{24a}$$

$$\text{s.t.} : \quad \forall\, i = 1 \cdots N,\; k = 1 \cdots V_j,$$

$$H_i^j \begin{bmatrix} g_i^k \\ -1 \end{bmatrix} \leq S_j(\Delta_i), \tag{24b}$$

$$\sum_{i=1}^{N} r_i^k d_i^k \geq y_j^k z_j^k. \tag{24c}$$

Here, Eq. 24a is the quadratic cost assigned to displacement in power of generator i. Eq. 24b constrains the generator i variables to be within the sub-polytope space. While, Eq. 24c is the power balance constraint. The result of the optimization problem are allocated vertices given as $[P_i^j \; r_i^k \; d_i^k]$. A polytope encloses the allocated vertices of each generator.

C. Scalability

The formulation in Sec. III-A is similar to that of the Optimal Power Flow (OPF) problem [24]. The time complexity in solving OPF can be attributed to the problem size and the solver used. Primal Dual Interior Point method is used to solve Eq. 23. In Sec. III-B, Eq. 24 is the function of number of inputs (N) and their size (resource capability envelope). An addition of a generator adds $\sum_{j=1}^{C} V_j$ constraints to the problem. Eq. 24b restrict the vertex (g_i^k) assigned to a generator within its envelope. The size of $S_j(\Delta_i)$ defines the search space and influences the computational time. However, it is independently applied for each generator. Thus, the complexity of this equation increases linearly with N. The coupling between generators appears as a linear combination in Eq. 24c and it scales accordingly. The structure of this constraint is bilinear. Hence, branch and bound algorithm is used to solve Eq. 24.

IV. Results

A. Test Case Data

The microgrid test-case is based on CIGRE MV benchmark [19], [20], European configuration. The network is modified to include distributed generation as shown in Fig. 3. The transmission line parameters and the nominal load data can be seen in Appendix C of [25].

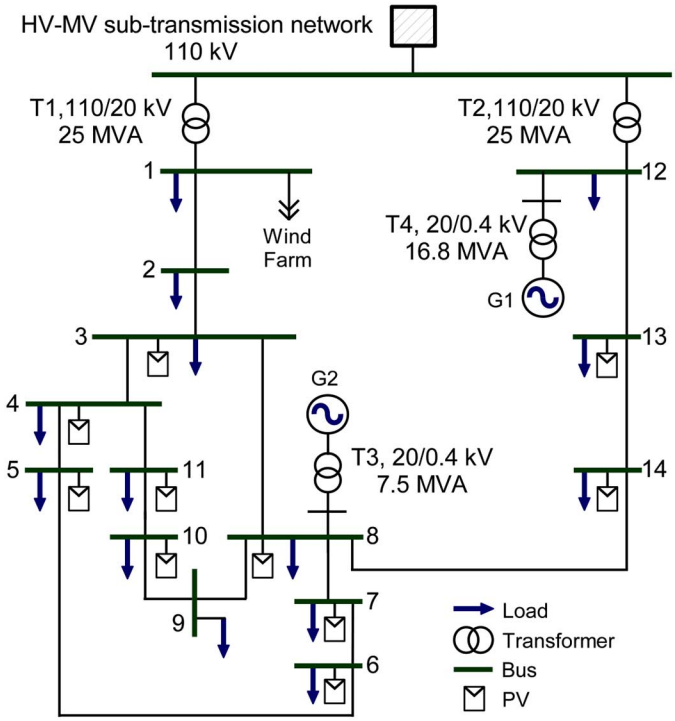

Fig. 3. CIGRE MV distribution network [19] modified as microgrid.

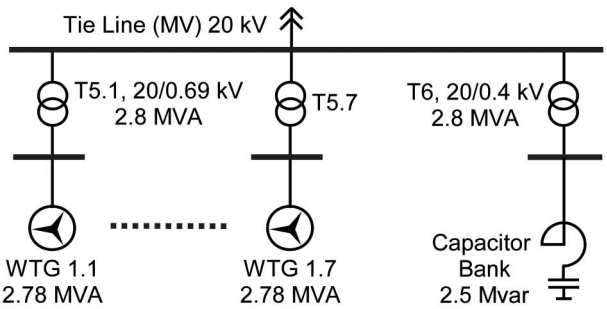

Fig. 4. Wind farm model.

A wind-farm consisting of 7 wind turbines is connected to MV network by a tie-line shown in Fig. 4. Each wind turbine is rated 2.78 MVA and operated at 0.9 power factor. The wind turbines are connected by a step-up transformer of equal ratings to 20kV bus. A capacitor bank is installed to improve the power factor. A wind farm controller allocates the reactive power to each wind turbine based on the overall active power generation at the tie-line. The probabilistic model of wind power output is derived from the historical time-series data using Alg. 1.

The load buses in the MV network are equipped with PV generation as shown in the Fig. 3. The nominal apparent power rating of the PV connected to each bus is given in Table I.

Two generators are connected to bus 8 and 12. They are operated by natural gas and provide necessary backup during the islanded mode operation of microgrid. In the grid-connected mode, they contribute to the demand and ancillary

TABLE I
PV DATA (S_{nom} [KVA], POWER FACTOR = 0.8)

Bus	S_{nom}	Bus	S_{nom}	Bus	S_{nom}	Bus	S_{nom}
1	3103	5	113.7	8	91.8	12	3129.4
3	78.5	6	85.7	10	174.67	13	5.32
4	69.6	7	12.0	11	51.6	14	84.4

TABLE II
SYSTEM DATA

		Gen. 1	Gen. 2	Grid
Incremental operating cost	b_i [\$/kWh^2]	0.04	0.038	0.1
	a_i [\$/kWh]	10	13	18
$\overline{P_i}$ [MW]		10	5	35
$\underline{P_i}$ [MW]		1	0.5	0
Temperature power slope (k_i) [°F/kW]		0.068	0.2066	-
Thermal stress up limit (H_i) [°F]		200	250	-
Thermal stress down limit (L_i) [°F]		-210	-270	-
Thermal time constant (τ_i) [min]		50	30	-
Maximum ramp-up rate (UR_i) [MW/h]		5.05	2.80	20
Maximum ramp-down rate (LR_i) [MW/h]		5.30	3.02	20

services requirements. The thermal generation cost (T) is 3.45 [\$/MMbtu]. The operational cost is given as,

$$\text{Cost}(P_i) = \text{Heat rate}(P_i) \times T\ , \tag{25a}$$

$$\text{Heat rate}(P) = a_i P_i + b_i P_i^2\ . \tag{25b}$$

The cost coefficients (a_i, b_i) are derived by fitting a second order polynomial to the historical data of generator output power vs. heat rate. The generator specifications are given in Table 2.

The dynamic ramp-rate limits of generators are derived using the approach discussed in Sec. II-D. However, static ramp-rate limits are considered for the power exchange with the HV grid.

The peak values $[P_{\min} \quad P_{\max}]$ for the demand are $[10 \ \ 41]$, power from the wind-farm $[6 \ \ 17]$ and PV $[0 \ \ 7]$ in MW. The historical data of power from wind-farm and PV is obtained from [26] and for load from [27]. It is normalized with respect to the use-case ratings.

B. Uncertainty Modeling

For a day ahead forecast, Alg. 1 is applied to generate S uncertainty realizations. Eq. 7 with the parameters $\beta = 10^{-4}, \epsilon = 0.1$ and $n_\delta = 1$ is used to generator 162 scenarios. Fig. 5 shows the % error with respect to the forecast level. Significant variation of error is observed along the forecast level hence validating the clustering approach. A binning strategy is used to categorize the error values in each cluster. The eCDF of forecast error in each cluster is obtained and used in method as discussed in Alg. 1.

The spatial diversity of uncertainty in the power balance is shown in Fig. 6. Here, various levels of uncertainty defines the percentage deviation from the forecast value. The temporal correlation is modeled by a second order Markov chain as discussed in Sec. II-B and is shown in Fig. 7.

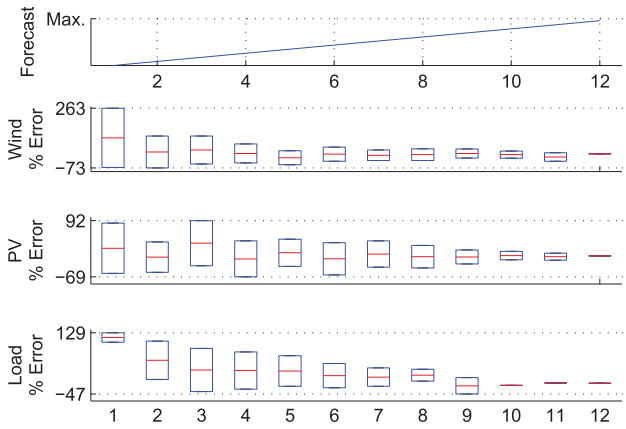

Fig. 5. The forecast level of each variable is divided into 12 levels. The figure shows % error of the stochastic variables obtained by sampling the eCDF of each forecast cluster S times. This diversity in error limits validates the clustering approach adopted in Alg. 1.

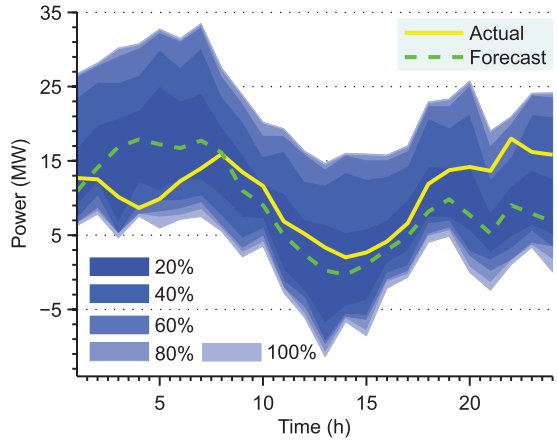

Fig. 6. The levels of uncertainty shows the % deviation of the uncertain power balance realizations from the day ahead forecast in the microgrid. The width of each level corresponds to the probability of occurrence of error. The result is based on the Monte Carlo simulations performed S times.

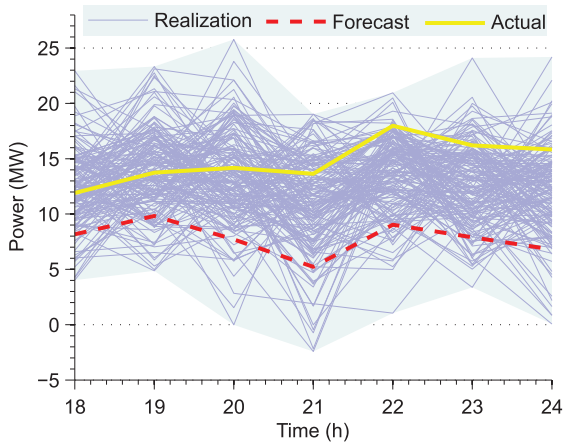

Fig. 7. The graph shows horizontal correlation between the power balance states as obtained by second order Markov chain. The *actual* curve is likely to follow the forecast trends with a certain probability that is the function of S and the order of Markov chain.

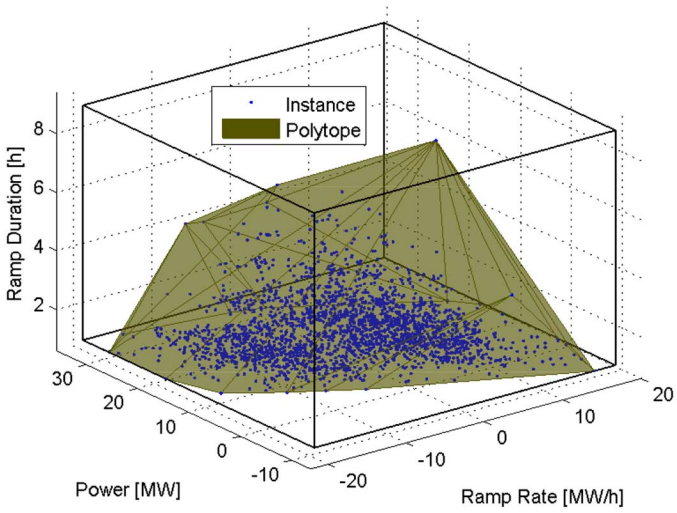

Fig. 8. A convex polytope encloses the points with its surface representing the worst case scenario. A BB is plotted for comparison with the polytope. It shows that substantial volume of the uncertain region can be reduced by the polytope approximation.

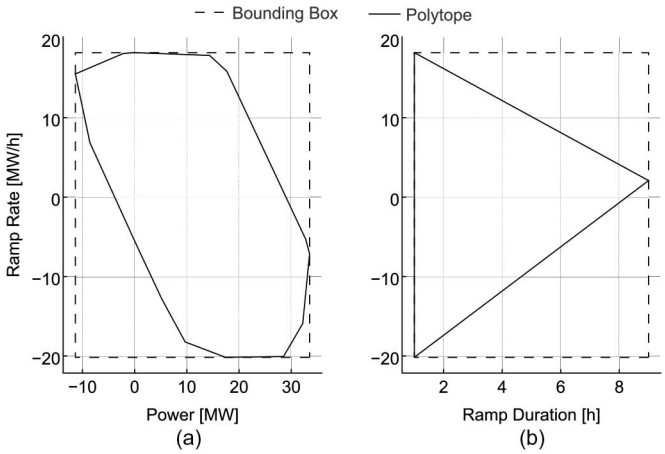

Fig. 9. This figure shows the projections of polytope and BB on $x-y$ and $y-z$ axes. (a) The ramp-rate requirement is shown as function of the power with lower demand experiencing higher ramp-up rate. Maximum ramp-down rate of 20 MW/h is probable at the capacity of 20 to 30 MW. While the ramp-up rate can get a maximum value of 18 MW/h when the demand is between -2 and 16 MW. (b) This graph shows a relationship between the ramp-duration and ramp-rate. Small values of ramp-rate are likely to be more sustained then large values.

C. Polytope Formulation

In this section the SDA from Sec. II-C is applied to the power balance dynamics obtained from the previous section. A convex polytope encloses the pivot-points as shown in Fig. 8. Fig. 9 shows the projections of polytope. It analyzes the ramp-rate and corresponding ramp-duration requirement at different power levels. It cannot be used for the volume comparison of polytope and BB as the projections are obtained while viewing the axes perpendicularly.

In [11], Dvorkin *et al.* have used a hyper-rectangular surface enclosing the points. The comparison of hyper-rectangle and polytope in Fig. 8 shows that volume of the polytope is 73.53 % less than that of the hyper-cube. The hyper-cube approach

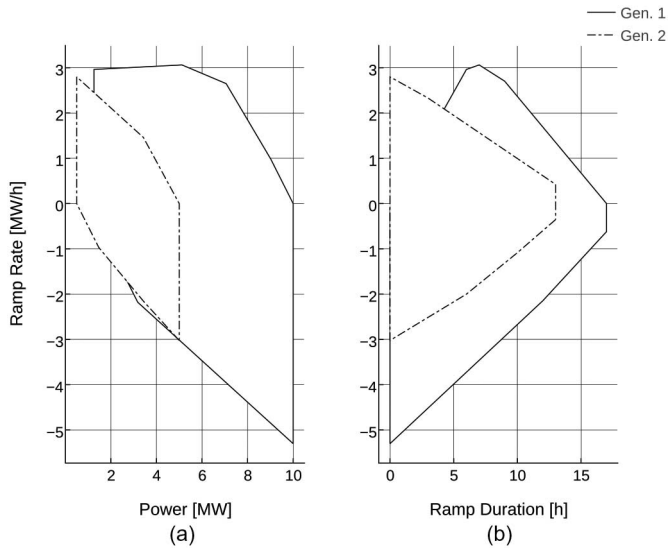

Fig. 10. Fig. (a) and (b) shows the $x-y$ and $y-z$ projections of the allocation of Δ among Gen. 1 and 2. The allocated capability is bounded by the operational constraints of each generator.

reflects maximum ramp-rate and the ramp-duration requirements for a given capacity and leads to conservative results. The comparison indicates significant reduction in the capability requirements can be achieved by using tighter approximation while still full-filling the probabilistic guarantees as discussed in Eq. 7. The confidence against uncertainty can be increased by decreasing the values of ϵ and β. It shall result in higher number of scenarios leading to increase in the space bounded by polytope. The demand polytope Δ is obtained by intersecting the polytope from Fig. 8 with the hyper-space extending along the positive power axis. It is then sectioned using Alg. 2 leading to a polygon $S_j(\Delta)$ for each demand value x_j along the power axis.

The dynamic ramp-rate of a generator is modeled using thermal stress model as discussed in Sec. II-D. The result is a polytope Δ_i for each generator. The power import capability polytope has a cubic structure due to the consideration of static ramp-rate limits defined by the ratings of HV/MV transformer. After modeling of the resource envelopes, the next step is the allocation process.

D. Polytopic Decomposition

As discussed in Sec. III, the decomposition of Δ is performed in two steps. In the first step, the demand x_j is dispatched by solving Eq. 23. The process is repeated C times. In the second step, each vertex of the polygon $S_j(\Delta)$ for the j^{th} demand is allocated by solving optimization problem in Eq. 24. The process results in the vertex assignment to generation resource i given as $[P_i^j \; r_i^k \; d_i^k]$. It is repeated for the j^{th} demand values and the k^{th} vertex of the polygon $S_j(\Delta)$. As a result of this process the spaces are allocated to each generation resource.

Fig. 10 shows the allocation among local generators in the microgrid. The optimization of individual polytope is based on the production cost while considering the operational constraints. Fig. 11 shows the envelope assigned to the power

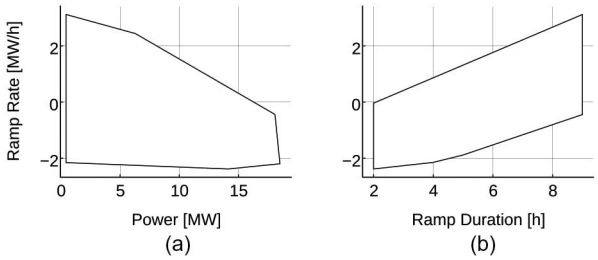

Fig. 11. This figure shows the (a) $x - y$ and (b) $y - z$ projections of the polytope assigned to power import from main grid. It provides a reference for the resource planning in the microgrid.

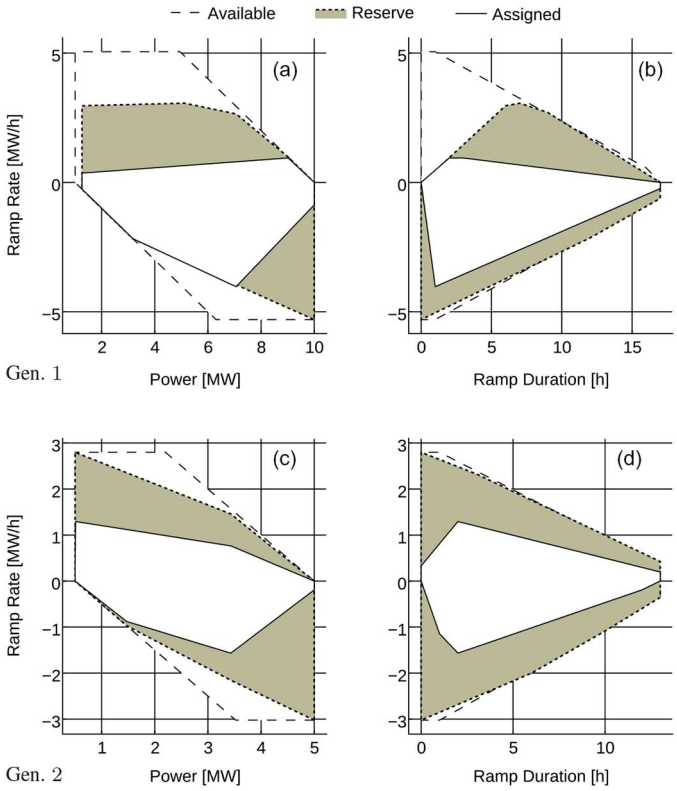

Fig. 12. The figure shows the projections of polytopes assigned to Gen. 1 and 2. The "assigned" areas are the generator polytopes against day-ahead demand forecast. The allocated polytopes Δ_i includes both the "assigned" and the "reserve" areas. While the "available" region shows the capability polytopes of generators. The space between "reserve" and "available" marks the un-used dynamic capability of a generator.

import from the main grid. It can be used in the resource planning for the islanded-mode operation of microgrid. Such that the fast and slow ramping units can be allocated with associated ramp duration capability.

Fig. 12 provides an insight in the capability utilization of Gen. 1 and 2. The projections of enclosed polytopes shows the comparative analysis of demand and reserve allocation among generators. The approach provides insights into the assigned, reserve and the available capabilities. It can be extended to the contingency reserve planning in microgrid. In case of a generator contingency the respective capability envelope shall be allocated among the remaining resources in a similar way. The

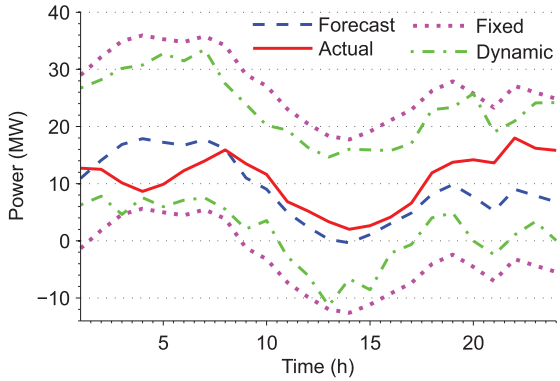

Fig. 13. Comparison of the reserve requirements for the day-ahead fixed and the dynamic range based approaches. It shows that the reserve requirement can be decreased while still covering the uncertainty with a probability defined in Eq. 7.

transmission line and bus contingencies can be incorporated during the allocation process as discussed in Sec. III-A.

E. Cost Analysis

In [28], authors have used maximum deviation from the day-ahead forecast as a reserve reference for the scheduling of up and down-spinning reserves. This approach assumes fixed uncertainty at all power levels. However, the proposed approach allows for the consideration of dynamic value of the uncertainty. It is obtained from the worst case limits of the power balance scenarios generated by the Monte Carlo simulations. Fig. 13 compares the limits associated with the fixed and dynamic reserve allocation approaches. The result shows 27 % reserve requirement can be reduced by dynamic dispatch of reserves as compared to fixed percentage of load ramp-up/down reserve approach.

V. Conclusion

Maintaining adequate reserve is essential for secure operation of the microgrid. In this paper, Monte Carlo simulations are used to obtain the uncertain power balance scenarios. The first order dynamics of these scenarios are modeled as instances in the space. A polytopic envelope compactly enclose these points providing a mechanism of the uncertainty quantification. The polytope represents overall demand and its uncertainty in the microgrid. In relevance, the capability envelopes of the generators are modeled with dynamic ramp-rate consideration. The demand polytope is then optimally allocated among the generator capability envelopes based on the incremental cost. This step allocates the dynamics of demand and reserves against forecast uncertainty. The result is an economic allocation of the reserve capability among the resources. In addition, the envelope assigned to the power import from the grid facilitate the resource planning in microgrid with the dynamics under consideration. In the end, a comparison of fixed vs dynamic reserve allocation in a standard day-ahead dispatch reflects the economic improvements. The proposed approach can be extended

to model the inter-dependency of demand and resource capabilities. Other resources like electric vehicles, storage and demand-side models can be incorporated in this regard.

REFERENCES

[1] A. M. Annaswamy and M. Amin, *IEEE Vision for Smart Grid Controls: 2030 and Beyond*, Jun. 2013, pp. 1–168.

[2] N. Hatziargyriou, Ed., *Microgrids: Architectures and Control*, 1st ed. Hoboken, NJ, USA: Wiley/IEEE Press, Mar. 2014.

[3] M. Nehrir *et al.*, "A review of hybrid renewable/alternative energy systems for electric power generation: Configurations, control, and applications," *IEEE Trans. Sustain. Energy*, vol. 2, no. 4, pp. 392–403, Oct. 2011.

[4] T. Vandoorn, J. Vasquez, J. De Kooning, J. Guerrero, and L. Vandevelde, "Microgrids: Hierarchical control and an overview of the control and reserve management strategies," *IEEE Ind. Electron. Mag.*, vol. 7, no. 4, pp. 42–55, Dec. 2013.

[5] A. Zakariazadeh, S. Jadid, and P. Siano, "Smart microgrid energy and reserve scheduling with demand response using stochastic optimization," *Int. J. Elect. Power Energy Syst.*, vol. 63, pp. 523–533, 2014.

[6] X. Yan, B. Francois, and D. Abbes, "Operating power reserve quantification through PV generation uncertainty analysis of a microgrid," in *Proc. IEEE Eindhoven PowerTech*, 2015, pp. 1–6.

[7] G. Papaefthymiou and B. Klockl, "MCMC for wind power simulation," *IEEE Trans. Energy Convers.*, vol. 23, no. 1, pp. 234–240, Mar. 2008.

[8] A. Kusiak and W. Li, "Short-term prediction of wind power with a clustering approach," *Renew. Energy*, vol. 35, no. 10, pp. 2362–2369, 2010.

[9] K. Margellos, P. Goulart, and J. Lygeros, "On the road between robust optimization and the scenario approach for chance constrained optimization problems," *IEEE Trans. Autom. Control*, vol. 59, no. 8, pp. 2258–2263, Aug. 2014.

[10] Y. Makarov *et al.*, "Integration of wind generation and load forecast uncertainties into power grid operations," in *Proc. IEEE PES Transmiss. Distrib. Conf. Expo.*, Apr. 2010, pp. 1–8.

[11] Y. Dvorkin, D. S. Kirschen, and M. A. Ortega-Vazquez, "Assessing flexibility requirements in power systems," *IET Gener. Transmiss. Distrib.*, vol. 8, pp. 1820–1830, Nov. 2014.

[12] M. Bucher, S. Chatzivasileiadis, and G. Andersson, "Managing flexibility in multi-area power systems," *IEEE Trans. Power Syst.*, 2015, to be published.

[13] W. Wei, F. Liu, and S. Mei, "Real-time dispatchability of bulk power systems with volatile renewable generations," *IEEE Trans. Sustain. Energy*, vol. 6, no. 3, pp. 738–747, Jul. 2015.

[14] F. Chernousko, "What is ellipsoidal modelling and how to use it for control and state estimation?," in *Whys and Hows in Uncertainty Modelling*, I. Elishakoff, Ed. New York, NY, USA: Springer, 1999, vol. 388, pp. 188–127.

[15] J. K. Delson, "Thermal stress computation for steam-electric generator dispatch," *IEEE Trans. Power Syst.*, vol. 9, no. 1, pp. 120–127, Feb. 1994.

[16] Z. Li and M. Shahidehpour, "Generation scheduling with thermal stress constraints," *IEEE Trans. Power Syst.*, vol. 18, no. 4, pp. 1402–1409, Nov. 2003.

[17] J. Jorgensen, S. Sorensen, K. Behnke, and P. B. Eriksen, "Ecogrid EU—A prototype for european smart grids," in *Proc. IEEE Power Energy Soc. Gen. Meeting*, 2011, pp. 1–7.

[18] Y. Guo and W. Gawlik, "A survey of control strategies applied in worldwide microgrid projects," in *Proc. Tagungsband ComForEn*, 2014, p. 47.

[19] K. Strunz *et al.*, "Benchmark systems for network integration of renewable and distributed energy resources," *Preliminary Version, Cigre Task Force C6*, 2009.

[20] D. Olivares, C. Canizares, and M. Kazerani, "A centralized energy management system for isolated microgrids," *IEEE Trans. Smart Grid*, vol. 5, no. 4, pp. 1864–1875, Jul. 2014.

[21] D. Barr, "The use of a data historian to extend plant life," in *Proc. IET Conf.*, Jan. 1994, pp. 35–39.

[22] G. M. Ziegler, *Lectures on Polytopes*. New York, NY, USA: Springer, 1995, vol. 152.

[23] M. De Berg, M. Van Kreveld, M. Overmars, and O. C. Schwarzkopf, *Computational Geometry*. New York, NY, USA: Springer, 2000.

[24] S. Frank, I. Steponavice, and S. Rebennack, "Optimal power flow: A bibliographic survey I," *Energy Syst.*, vol. 3, no. 3, pp. 221–258, 2012.

[25] K. Skaloumpakas, "Response of low voltage networks with high photovoltaic systems penetration to transmission network faults," M.S. thesis, Intelligent Electrical Power Grids, TU Delft, Delft Univ. Technol., Delft, The Netherlands, 2014.

[26] TenneT-TSO. "Network data," 2015, data for 2013–2014 [Online]. Available: http://www.tennettso.de

[27] 50-Hertz. "Forecast control area load," 2015, data for 2013–2014 [Online]. Available: http://www.50hertz.com

[28] M. Vrakopoulou, K. Margellos, J. Lygeros, and G. Andersson, "A probabilistic framework for reserve scheduling and N-1 security assessment of systems with high wind power penetration," *IEEE Trans. Power Syst.*, vol. 28, no. 4, pp. 3885–3896, Nov. 2013.

Sohail Khan (S'14) received the B.S.E.E. degree from the CIIT, Islamabad, Pakistan, and the M.S.E.E. degree from NUST, Islamabad, Pakistan, in 2008 and 2010, respectively. Currently, he is pursuing the Ph.D. degree at Vienna University of Technology, Vienna, Austria. He is also a Research Fellow at Complex Energy Systems, Department of Energy, Austrian Institute of Technology, Vienna, Austria. Previously, he was a Lecturer with Electrical Engineering Department, CIIT, Islamabad, Pakistan and HITEC, Taxila, Pakistan. Before that, he was a Junior Engineer at Nautica Group, Islamabad, Pakistan. His research interests include microgrids, distribution system automation and operations research.

Wolfgang Gawlik received the Dipl.-Ing. degree in 1997 and the Dr.-Ing. degree in 2004 from the University of Erlangen-Nuremberg, Germany. Currently, he is a Full Professor for energy systems technology at TU Wien, Vienna, Austria. Before that, he was a Senior Key Expert System Dynamics and Senior Project Manager at Siemens Power Technologies International, Berlin, Germany. His research interests include supergrids, smart grids/microgrids and electromobility, universal grids and software for network analysis, planning and steady state and dynamic modeling. He is active in national and international working groups and member of CIGRE Austria, OVE, and VDE.

Peter Palensky (SM'06) received the M.S.E.E., the Ph.D., and the Habilitation degrees from Vienna University of Technology, Vienna, Austria, in 1997, 2001, and 2015, respectively. Currently, he is a Professor for intelligent electric power grids at TU Delft, Delft, The Netherlands. Previously, he was a Principal Scientist for complex energy systems and Head of Business Unit "Sustainable Building Technologies" at the Austrian Institute of Technology, CTO of Envidatec Corp., Hamburg, Germany, an Associate Professor with the Department of Electrical, Electronic and Computer Engineering, University of Pretoria, Pretoria, South Africa, a University Assistant at the Vienna University of Technology, Vienna, Austria, and Researcher with the Lawrence Berkeley National Laboratory, Berkeley, CA, USA. His research interests include complex energy systems and smart grids. He is active in international committees like ISO, IEEE, and CEN.